Indian Journal of Geo-Marine Science
Vol. 45(2), February 2016, pp. 261-268

# A numerical approach for understanding the temporal and spatial correlation scales of sound velocity in long term: a case study for the source and surrounding region of the Kuroshio Current

Lianglong Da, Wuhong Guo* & Weihua Li
Department of Navigation Observation, Navy Submarine Academy of Chinese People's Liberation Army, Qingdao 266071, China
*[Email: guowuhongcn@163.com]

*Received 12 May 2014; revised 05 November 2014*

To accurately understand the temporal and spatial distributions of sound velocity fields and their relevant characteristics, numerically investigated the sound velocity auto-correlation index at the source and adjacent region of the Kuroshio Current using 1911-2001 observation data. Auto-correlation index was fitted using a Gaussian function for the temporal and spatial scales of the investigated regions. The correlation scales in time and spatial domain in spring, summer, fall, and winter were 14.2/145.3, 14.2/135.9, 13.5/133.8, and 13.7/143.3 days/km, respectively. These scales are applied to the reconstructed sound velocity model in terms of empirical orthogonal functions. The error of the sound velocity constructed was minimal (3 m/s) compared with those constructed using other methods (up to 4.3 m/s). This method improves the precision of the sound velocity reconstruction compared with that based on monthly data. The use of temporal and spatial scales enhances the accuracy of sound velocity reconstruction.

**[Keywords**: sound velocity profile; auto-correlation index; correlation scale; Kuroshio source region]

## Introduction

Oceans have great temporal and spatial variation. Studies of oceans and other related fields involve a large amount of data with a varying distribution over time and space. Because some of the data are not continuous or sufficient, related studies often suffer from sizeable errors or even incorrect results. Therefore, effectively utilizing temporal and spatial data is of great concern in the fields of geography, astronomy, oceanography, and economics, among others[1,2]. Reasonable selection of temporal and spatial scales is particularly important in sound velocity reconstruction with measured data.

Temporal and spatial autocorrelation analysis can be used for the analysis and calculation of temporal and spatial correlations between datasets, thereby better describing the temporal and spatial distribution of oceanic data. The concept of spatial autocorrelation was first proposed by Moran in 1950 to calculate the degree of resemblance between cell attribute values in spatially adjacent regions[3]. Cliff and Ord conducted pioneering work in spatial statistics[4], establishing the preliminaries for the theoretical structure of this field. Anselin laid foundations for the development and perfection of temporal and spatial statistics and applied his approach to the field of economics[5]. Lee proposed a temporal and spatial auto-correlation index by combining the Pearson correlation coefficient and the Moran auto-correlation index, based on previous studies by others[6]. According to this study, the temporal and spatial auto-correlation index refers to the index that describes the interdependence among the observed data of certain variables within the same distribution area and within the same time period. Susan *et al.* applied extracted temporal and spatial auto-correlation scales to the OTIS data assimilation system, which improved the system's effectiveness in offshore areas[7]. Starkar *et al.* performed a temporal auto-correlation analysis of sequential sea surface wind stress and wave height data and extracted temporal scale information, improving the data assimilation effectiveness of numerical models[8,9]. Cao *et al.* studied county-scale economics based on a spatial model using spatial auto-correlation coefficients[10]. Josey *et al.* demonstrated the impact of sea surface heat data on atmospheric models at different scale regions of the Mediterranean Sea[11]. Nikolaos *et al.* studied the decadal-scale variability of sea surface temperature in the Mediterranean Sea in relation to atmospheric variability[12]. Byung *et al.* used a seasonal ARIMA model in Mongolia to

evaluate temporal-spatial precipitation variability and predictions[13].

However, most current applications of sea sound velocity fields involve grid and monthly average data. In the time dimension, tradition methods use monthly means based on the monthly separation of data. Moreover, the spatial dimension is based on gridding. The data obtained based on traditional methods have two limitations: (1) Temporal dimension disadvantage: the monthly average data are still used when the analyzed point is at the beginning or end of the month. (2) Spatial dimension disadvantage: the average coordinate grid data are still applied when the analyzed point is within a coordinate grid but far from the center of the grid.

To solve these problems, our research calculated the auto-correlation index of the Kuroshio Current source and adjacent region. Temporal and spatial correlation scales of the Kuroshio source and adjacent region were acquired through a Gaussian function. We reconstructed sound velocity sections in different temporal and spatial scopes for comparison to demonstrate the superiority of the proposed method.

**Materials and Methods**

Kuroshio is a strong Pacific western boundary current. It originates from the north branch of the North Equatorial Current in the Philippine Sea and goes from the east coast of Taiwan into the East China Sea. It then flows northeast along the Okinawa Trough[14,15]. The observation data used in this paper are from CTD data, Nansen data, ARGO data, and other data between 1911 and 2001 that were collected by the National Marine Data and Information Service of China (http://www.soa.gov.cn/zwgk/bjgk/jsdw/gjhyxxzx/). These data include 14,827 observation sections in the Kuroshio source and adjacent region, and the measurement depths vary according to ocean regions. The positional distribution is shown in Fig. 1, and the time distribution is shown in Fig. 2 (observation frequencies varied in different years (with no observations in some years)). Distribution of the observation positions given by Fig. 1 covers the Kuroshio source and adjacent region. Figs. 1 and 2 indicate that the distribution of the observations is not even. Thus, the data must be temporally and spatially pretreated.

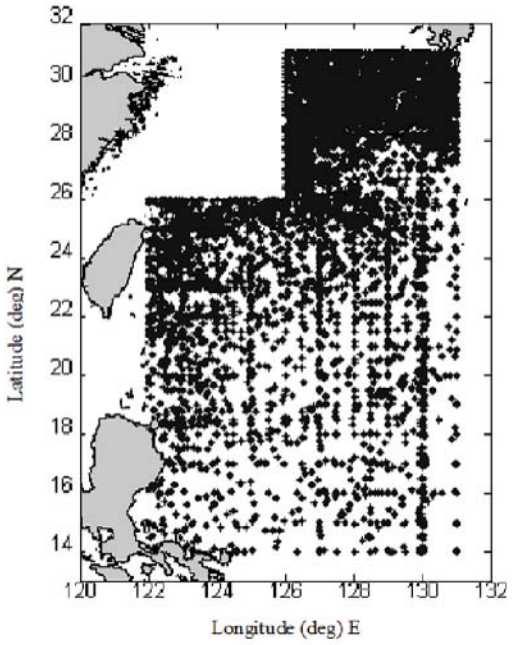


Fig. 1--Distribution of the observation data in the Kuroshio source and adjacent region

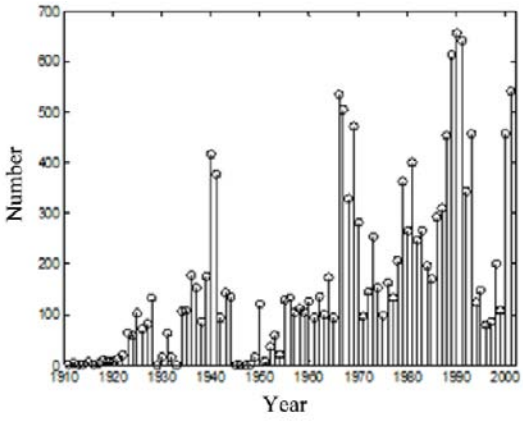


Fig. 2--Distribution of the observation data according to year

To obtain the statistics of the sound velocity section in the source and adjacent region of Kuroshio over time and space, the time should first be divided based on the season. Second, the auto-correlation index should be investigated according to this division. We set April, May, and June as spring; July, August, and September as summer; October, November, and December as fall; and January, February, and March as winter[16], and the observation data were separated into these different seasons. Table 1 lists the number of observations in each season.

Table 1--Number of observations for each of the four seasons

| Season | Number of observations |
|---|---|
| Spring | 3,734 |
| Summer | 4,111 |
| Fall | 3,345 |
| Winter | 3,637 |

The calculation of the sound velocity auto-correlation index by the average monthly dataset will be discussed below. The grid resolution is 30'×30'. Therefore, the observation data can be interpolated horizontally and vertically using the minimum spline criteria to construct the monthly average sound velocity field.

**Auto-correlation index of the measured sound velocity data**

*Auto-correlation index algorithm*

To calculate the observed sound velocity factor $\Psi$, we must find the grid data point $\overline{\Psi}$ that is closest to $\Psi$ among the 30'×30 monthly average grid data. Next, the anomalies of every $\Psi$ in the observation dataset are calculated: $\Psi' = \Psi - \overline{\Psi}$. The other anomaly is $\Psi''$. Any two anomalies $\Psi'$ and $\Psi''$ can compose a data pair $(\Psi', \Psi'')$ when the space distance L and time interval T of two data points in the data pair satisfy the following conditions:

$$\begin{aligned} &m\Delta r - \Delta r_0 \le L \le m\Delta r + \Delta r_0 \\ &\Delta r = 10km, \Delta r_0 = 5km \\ &n\Delta t - \Delta t_0 \le T \le n\Delta t + \Delta t_0 \\ &\Delta t = 1day, \Delta t_0 = 0.5day \end{aligned} \tag{1}$$

These conditions represent the data pair in one cell, $bin(m,n)$, where $m = 0,1,2,...,30$ is the spatial span and $n = 0,1,2,...,30$ is the time span.

After the observation factor is divided into scaled cells according to time and space, the auto-correlation index of the observation factor can be calculated from the following formula[16]:

$$\eta(m,n) = \frac{\sum_{bin(m,n)} \Psi'\Psi''}{\sum_{bin(m,n)} [\Psi']^2 \sum_{bin(m,n)} [\Psi'']^2} \tag{2}$$

The observed sound velocity is calculated from the following formula:

$$c = 1449.22 + \Delta c_T + \Delta c_S + \Delta c_P + \Delta c_{STP}$$

where

$$\Delta c_T = 4.6233T - 5.4585\times10^{-2}\times T^2 + 2.822\times10^{-4}\times T^3 - 5.07\times10^{-7}\times T^4$$

$$\Delta c_S = 1.391\times(S-35) - 7.8\times10^{-2}\times(S-35)^2$$

$$\Delta c_P = 1.6051\times10^{-1}\times P + 1.0279\times10^{-5}\times P^2 + 3.451\times10^{-9}\times P^3 - 3.503\times10^{-12}\times P^4$$

$$\begin{aligned} \Delta c_{STP} = {} & (S-35)\left[-1.197\times10^{-3}\times T + 2.61\times10^{-4}\times P - 1.96\times10^{-1}\times P^2 - 2.09\times10^{-6}\times PT\right] \\ & + P\left[-2.796\times10^{-4}\times T + 1.3302\times10^{-5}\times T^2 - 6.644\times10^{-8}\times T^3\right] \\ & + P^2\left[-2.391\times10^{-1}\times T + 9.286\times10^{-10}\times T^2\right] - 1.745\times10^{-10}\times P^3 T \end{aligned}$$

Here, $T$ is temperature (°C), $S$ is salinity (‰), and $P$ is pressure (kg/cm$^2$).

The observation sound velocity profile has been standardized into divisions of 0, 5, 10, 15, 20, 25, 30, 35, 50, 75, 100, 125, 150, 200, 250, 300, 400, 500, 600, 700, 800, 900, 1,000, 1,500, 2,000, 3,000, 4,000, 5,000, and 6,000 m according to the standard pressure levels that are generally accepted in the field of oceanography. The observed data were obtained via interpolation when they were not on the same level. Hence, we can obtain the auto-correlation index for each layer in terms of the layer depth. Finally, the averaged results will be used.

*Calculation of the auto-correlation index*

To calculate the auto-correlation index of each season, the data should first be matched. The data pairs of the four seasons are shown in Fig. 3 based on Eq. (1).

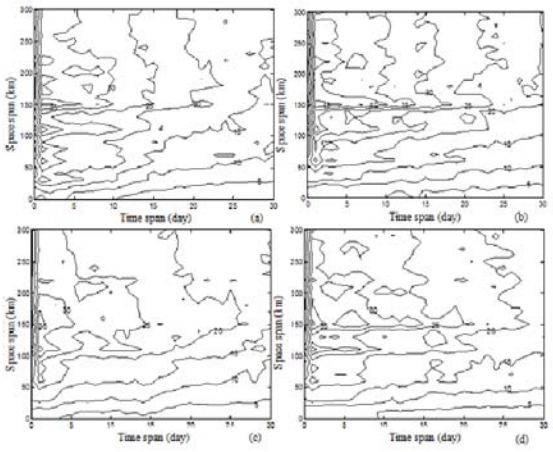


Fig. 3--Number of data pairs in each season: (a) spring, (b) summer, (c) fall, and (d) winter

Fig. 3 illustrates that there are at least 500 data pairs in each season. The sample size was much larger than those in literatures[16,17]. The auto-correlation index is an artificially constructed index that is used to reflect the correlative dependence between data at a certain position r and a certain time t with those at a different position r' and time t'. The auto-correlation index is calculated by Eq. (2) using the data pairs above, and the auto-correlation indices of the four seasons are shown in Fig. 4. The spatial and temporal spans of the four seasons are 300 km and 30 days, respectively. The contour interval is set in proportion to each 0.1 units of the auto-correlation index.

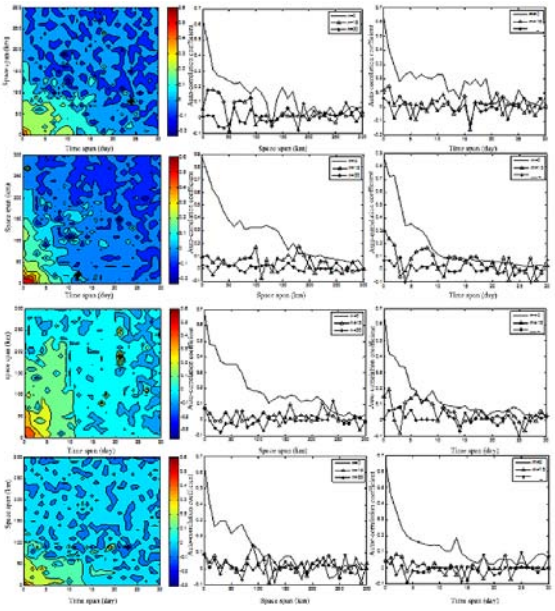

Fig. 4--Auto-correlation index changes along with the time and space spans (from top to bottom: spring, summer, fall, and winter)

The auto-correlation index of the four seasons changes with the time and space spans, as shown in Fig. 4 (left), and decreases gradually as the time and space spans increase, from approximately 0.6 to zero. Values of the auto-correlation index with changing space span are given for constant time spans of 0, 15, and 30 days to illustrate the variation of the auto-correlation index with the time and space spans (Fig. 4 (middle)). Furthermore, values of the auto-correlation index with changing time span is given for constant spatial spans of 0, 150, and 300 km (Fig. 4 (right)). Because the auto-correlation index possesses Gaussian characteristics[16,17], we will use a Gaussian function fitting for the temporal and spatial scales. P. C. Chu calculated the temporal and spatial correlation scales for all four seasons in the Chinese Yellow Sea using the United States Navy MOODS datasets[17]. The summer and winter results presented in his study are consistent with ours, and all of the results follow Gaussian distributions. However, our spring and fall results do not correspond with his, which instead display a transition feature. We observe that the depths of the Kuroshio source and adjacent region are greater than 100 m and are mainly affected by the Kuroshio Current[18], unlike the shallow Yellow Sea waters that P. C. Chu considered. This difference might be the main cause of the different results.

**Significance test of the auto-correlation index**

The auto-correlation index calculated within a spatial span of 300 km and a temporal span of 30 days and used in sound velocity profile reconstruction is appropriate for use. According to Eq. (2), the result yields an estimate of each data pair's auto-correlation index. We can use the t-distribution to validate the significance of the auto-correlation index with the following formula from Walpole and Myers (1989)[19]:

$$t = \frac{\eta\sqrt{P-2}}{\sqrt{1-\eta^2}} \tag{3}$$

$P$ is the number of data pairs in each cell, as shown in Fig. 3.

The significant test criterion $\eta_\alpha$ can be obtained by transforming Eq. (3) into

$$\eta_\alpha = \frac{t_\alpha}{\sqrt{P-2+t_\alpha^2}} \tag{4}$$

When the calculated auto-correlation index fits the condition $\eta(m,n) > \eta_\alpha$, it indicates that the calculated auto-correlation index meets the significance criteria (here, $\alpha = 0.1$). From Eq. (4), we can obtain the distribution of the criterion $\eta_\alpha$, which changes with the temporal and spatial spans, as shown in Fig. 5.

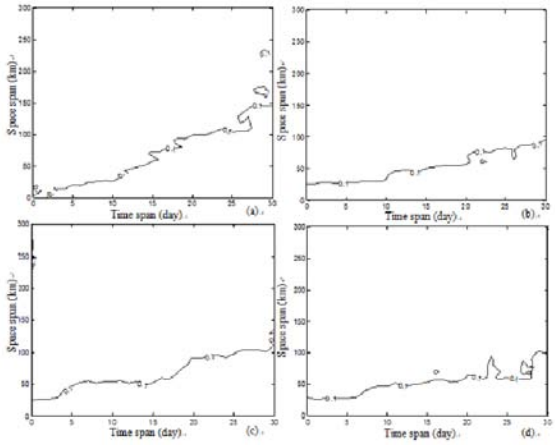

Fig. 5--Criterion (0.1 significance level) for the auto-correlation index significance test for (a) spring, (b) summer, (c) fall, and (d) winter

Fig. 5 illustrates that the significant test criteria of the auto-correlation index change with the seasons. We can obtain significant results for the auto-correlation index according to Figs. 4 and 5 and the significant test criteria, as shown in Fig. 6.

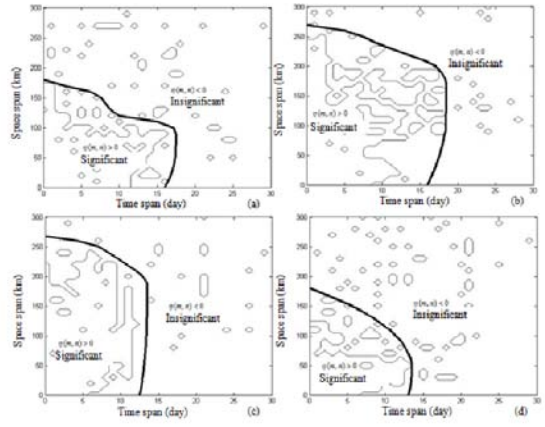

Fig. 6--Significance test of the auto-correlation index at a level of 0.1 for (a) spring, (b) summer, (c) fall, and (d) winter

Fig. 6 illustrates that there are many discrete points in the results of the four seasons, mainly because of insufficient data. Thus, a maximum-distance clustering method is applied to divide the data into two categories to make the regional division of significance clear[20,21&22]. Thick lines in the figure divide the significance test results into two categories. The figure shows that the 16 day/170 km, 16 day/240 km, 13 day/240km, and 13 day/170 km time-space scales exhibited satisfactory significance. These results can approximately explain the number of temporal and spatial correlation scales.

**Optimization algorithm of the temporal and spatial correlation scales**

The changes in the auto-correlation index exhibit Gaussian features, and thus, the auto-correlation index can be used for a Gaussian fitting function[16,17& 19].

$$\eta(m,n)=\eta(0,0)\exp[-A^2(m\Delta r)^2-C^2(n\Delta t)^2] \tag{5}$$

Applying Eq. (5) as a fitting function, data fitting is performed using the least-squares method, and the temporal and spatial correlation scales $A^{-1}$ and $C^{-1}$ of the different seasons can be derived from the fitted data. To validate the results, the hypothesis is tested based on the $F$ distribution:

Hypothesis $H_0$ : temporal and spatial correlation scales $A^{-1}$ and $C^{-1}$ are invalid;

Hypothesis $H_1$ : temporal and spatial correlation scales $A^{-1}$ and $C^{-1}$ are valid.

The test formula based on the $F$ distribution is

$$f=\frac{R/k}{E/(l-k-1)} \tag{6}$$

where $k=2$ , $l=31$ are the number of temporal and spatial scale cells and

$$R=\sum_m\sum_n\left[\ln\hat{\eta}(m,n)-\overline{\ln\eta(m,n)}\right]^2$$

$$E=\sum_m\sum_n\left[\ln\hat{\eta}(m,n)-\ln\eta(m,n)\right]^2 \tag{7}$$

When $f>f_\alpha(k,l-k-1)$ , Hypothesis $H_0$ does not hold but $H_1$ does hold, indicating that $A^{-1}$ and $C^{-1}$ are valid.

**Results and Discussion**

**Temporal and spatial correlation scale extraction**

To obtain the temporal and spatial correlation scale of the Kuroshio source and adjacent region and obtain the results of each season in the area, the temporal and spatial correlation scales $A^{-1}$ and $C^{-1}$ in Eq. (5) are calculated using Eq. (5) as the fitting function.

The values are shown in Table 2.

Table 2--Temporal and spatial correlation scales of each season

| Season | Temporal scale $C^{-1}$ ( day) | Spatial scale $A^{-1}$ (km) |
|---|---|---|
| Spring | 14.2 | 145.3 |
| Summer | 14.2 | 135.9 |
| Fall | 13.5 | 133.8 |
| Winter | 13.7 | 143.3 |

To validate the results, we test the temporal and spatial correlation scales based on the $F$ distribution with a confidence level of $\beta = 0.01$ and the testing value $f_{0.01}(2,28)=5.45$. If the result is larger than the testing value, the reliability of the result exceeds 99%. The detailed results are shown in Table 3.

Table 3--Results of the significance test for the correlation scales

| Season | Result of $F$ test | Conclusion |
|---|---|---|
| Spring | 19.1854 | valid |
| Summer | 22.4261 | valid |
| Fall | 20.1546 | valid |
| Winter | 17.4278 | valid |

The results indicates that using a Gaussian function to fit temporal and spatial correlation scales provides better results, and the F test result is considerably larger than the testing value, indicating that the temporal and spatial correlation scales are effective.

**Application of the temporal and spatial scales in sound velocity reconstruction**

The sound velocity profile changes significantly for different times and locations due to the influence of the Kuroshio current. To reconstruct the sound velocity profile more accurately, the temporal and spatial correlation scales are taken as the scope to extract the sound velocity profile according to the method of empirical orthogonal functions[23,24&25].

The data used here are from the East China Sea experiment that was performed on August 3, 1987. Fig. 7 presents the observed position and seafloor topography. Sections of the observation data are from 701 to 710 crossing the Okinawa Trough. Figure illustrates that the Okinawa Trough's terrain changes greatly and that the depth of the sea quickly changes from 200 to 900 m. Years of research have indicated that a perennial ocean front exists in the region[10].

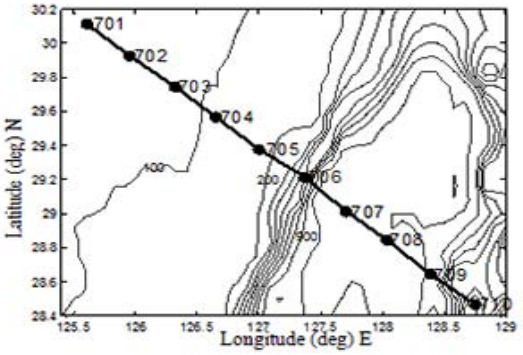


Fig. 7--Position and topography for 701-710 in the East China Sea

Sound velocity profiles are extracted from different temporal and spatial scopes to reconstruct the overall sound velocity profile, and the reconstruction results differ considerably. Fig. 8 presents the maximal margin between the reconstruction and observation profiles for different temporal and spatial scales. We sample 23 profiles to reconstruct the sound velocity in the 709 position from 36 profiles obtained every five days from 10 to 30 days and every 50 km from 100 to 300 km. Optimal space-time scope should use temporal and spatial correlation scales of 14.2 days/135.9 km in the summer, and the parameter should be rounded up, i.e., to 15 days/136 km, to include the spatial and temporal scales for a total of 24 profiles. Fig. 8 illustrates that the error of the result is minimized when reconstructed with 15 day/136 km, indicating that the temporal and spatial correlation scales are the optimal scope for reconstruction.

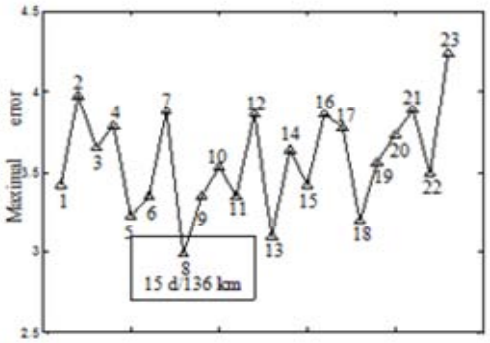


Fig. 8--Maximal error between the reconstructed and observed profiles for different temporal and spatial scales (1, 10 days/100 km; 2, 10 days/150 km; 3, 10 days/200 km; 4, 10 days/250 km; 5, 10 days/300 km; 6, 15 days/100 km; 7, 15 days/150 km; 8, 15 days/136 km; 9, 15 days/200 km; 10, 15 days/250 km; 11, 15 days/300 km; 12, 20 days/100 km; 13, 20 days/150 km; 14, 20 days/200 km; 15, 20 days/250 km; 16, 20 days/300 km; 17, 25 days/100 km; 18, 25 days/150 km; 19, 25 days/200 km; 20, 25 days/250 km; 21, 30 days/100 km; 22, 30 days/150 km; 23, 30 days/200 km)

From the above analysis of the sound velocity profile of 709 individual positions, the region easily forms an ocean front, and 10 sections from 701 to 710 points are obtained, as shown in Fig. 9. The background in Fig. 9 (a) and (b) is the observed sound velocity profile. Thick lines in (a) represent the sound velocity profile calculated from the monthly average data, and the thick lines in (b) represent the sound velocity profile derived from the reconstructed data. According to the observed data, there are two clear sound velocity fronts in the cross section; these fronts are located in the 703-704 and 706-707 regions and are represented by a black dotted line in the background in Figs. 9 (a) and (b). However, in Fig. 9 (a), the two sound velocity fronts are not distinct and the 703-704 region is nearly non-existent. The presence of the front can be observed in the 706-707 region, but the frontal width is too large. The blank regions in the figures represent the sea-floor topography. Because the grid points of the monthly average grid data are fixed, the results may not be consistent with the measured water depth data, and the isolines of the monthly average data have large confluence areas with the measured topographic sites.

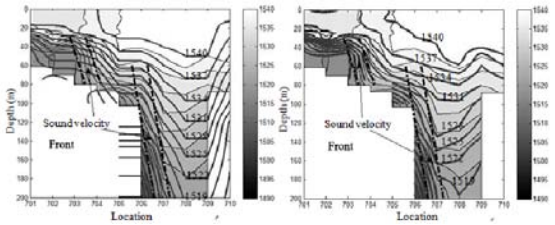


Fig. 9--Sound velocity section (background is the observation data). (a) Monthly sound velocity section. (b) Reconstructed sound velocity section

Sound velocity section obtained from the reconstruction data is presented in Fig. 9(b). In this section, the location and width of the sound velocity front are the same as the result given by Fig. 9(a), which is better than the result from the monthly average data and has a superior topographic match.

This study has a limitation. It did not consider chronological changes in sea temperature, salinity, and pressure over the past 90 years. These changes, particularly in temperature, have some influence on the calculation results in this study. Considering that this study focused on a different aspect, namely, the temporal and spatial correlation scales of the sound velocity, we will pay special attention to this issue in our future studies.

## Conclusion

Considering the problem that the sound velocity reconstruction in the Kuroshio source and adjacent region is not sufficiently accurate and given the weakness of the monthly average grid data, we calculated the auto-correlation index using temporal and spatial correlation scales with Gaussian function fitting. The following two important conclusions can be made from the application of this method:

Temporal and spatial correlation scales in the Kuroshio source and adjacent region are obtained using the observed oceanography data from 1911 to 2001. The correlation scales are as follows: spring, 14.2 days/145.3 km; summer, 14.2 days/135.9 km; fall, 13.5 days/133.8 km; and winter, 13.7 days/143.3 km. Scales are tested by t and F distributions. These results demonstrate that the temporal and spatial scales obtained by this method are effective. The summer spatial and temporal scales are used as the data scope and are applied to the sound velocity reconstruction model based on an improved empirical orthogonal function. After selecting 24 different scopes to reconstruct the sound velocity, the results illustrate that compared with when the monthly average data are used, a reconstruction that uses spatial and temporal scales is superior to other methods. Thus, sound velocity profile reconstruction using the data within the temporal and spatial correlation scales contains more information, which represents an improvement compared to sound velocity profile reconstruction using one-day or average data.

## Conflict of interest

The authors declare no conflict of interest.

## References

1. Meehl, G. A., Lukas, R., Kiladis, G. N., Weickmann, K. M., Matthews, A. J. & Wheeler, M., A conceptual frame work for time and space scale interactions in the climate system. *Climate Dynamics*, 17(2001): 753-775.

2. Lopez-Hernandez, F. A. & Chasco, Yrigoyen, Time-trend in spatial dependence: specification strategy in the first-order spatial autoregressive model. *Estudios de Economia Aplicada*, 25(2007): 631-650.
3. Moran, P. A. P., Notes on continuo us stochastic phenomena. *Biometrika*, 37 (1950): 17-23.
4. Cliff, A. & Ord, J. K., Spatial Processes: Models and Applications, (Pion, London) 1981.
5. Anselin, L. & Griffith, D., Do spatial effects really matter in regression analysis. *Regional Science Association*, 65(1988): 11-34.
6. Lee, S., Developing a bivariate spatial association measure: An integration of Pearson's r and Moran's I. *Journal of Geographical Systems*, 3 (2001): 369-385.
7. Wells, Susan K., *Temporal and spatial decorrelation scales of the Yellow Sea thermal fields*, (Naval Postgraduate School) 1994, pp. 1-115.
8. Abhijit Sarkar, Sujit Basu, A. K. Varma, & Jignesh Kshatriya, Auto-correlation analysis of ocean surface wind vectors. *Journal of Earth System Science*, 111(2002): 297-303.
9. Abhijit Sarkar, Jignesh Kshariya, & Satheesan, K., Auto-correlation analysis of wave heights in the Bay of Bengal. *Journal of Earth System Science*, 115(2006): 235-237.
10. Cao, F. D., Wu, J. & Xu, M., Research on spatial disparity of economy at county level based on the spatial econometrics mode. *Areal Research and Development*, 29(2010): 23-29.
11. Josey, S. A., Somot, S., & Tsimplis, M., Impacts of atmospheric modes of variability on Mediterranean Sea surface heat exchange. *J. Geophys. Res.*, 116(2012): C02032.
12. Nikolaos Skliris, Sarantis Sofianos, Athanasios Gkanasos, & Annda Mantzifou, Decadal scale variability of sea surface temperature in the Mediterranean sea in relation to atmospheric variability. *Ocean Dynamics*, 62(2012): 13-30.
13. Byung Sik Kim, Syed Zakim Hossein, & Gyewoon Choi, Evaluation of temporal-spatial precipitation variability and prediction using seasonal ARIMA model in Mongolia. *KSCE Journal of civil Engineering*, 15 (2011): 917-925.
14. Hinata, T., Seasonal variation and long-term trends of the oceanographic conditions along a fixed hydrographic line crossing the Kuroshio in the East China Sea. *Oceanogr. Mag.*, 45 (1996): 9-32.
15. Qiu, B. & Imasato, N., A numerical study on the formation of the Kuroshio Counter Current and the Kuroshio Branch Current in the East China Sea. *Cont. Shelf Res.*, 10(1990): 165-184.
16. Chu, P. C., Gui, W. & Chen, Y. C., Japan Sea thermohaline structure and circulation. *American Meteorological Society*, 32 (2002): 3596-3615
17. Chu, P. C., Wells, S. K., Heager, S. D., Szezechowski, C. & Carron, M., Temperal and spatial scales of the Yellow Sea thermal variability. *J. Geophys. Res.*, 102(1997b): 5655-5668.
18. Qiao, F. L., *Regional oceanography of China seas-physical oceanography*, (China ocean press, Beijing) 2012, pp. 191-197.
19. Walpole, R. E. & Myers, R. H., *Probability and Statistics for Engineers and Scientists*, 4th ed, (Macmillan, Indianapolis Ind.) 1989, pp. 765.
20. Hoje Kang, Detecting agglomeration processes using space-time clustering analyses. *The Annals of regional science*, 45(2010): 291-311.
21. Sun, H. Y., Wu, Z. & Fang, Z. B., Observation on warmer winter phenomena of China from the perspective of scan statistics. *Application of statistics and Management*, 27(2008): 952-958.
22. Youngho Kim & Morton O'kelly, A Bootstrap based space-time surveillance model with an application to crime occurrences. *Journal of Geographical Systems*, 10(2005):141-165.
23. Sun, C. & Watts, D., A circumpolar gravest empirical mode for the southern ocean hydrography. *J. Geophys. Res.*,106(2001): 2833-2856.
24. Park, J. C. & Kennedy, R. M., Remote Sensing of Ocean Sound speed profiles by a perception Neural network. *IEEE J. Ocean Eng.*, 12(1996): 216-224.
25. Pascual, A., & Gomis, D., Use of surface data to estimate geostrophic transport. *J. Atmos Oceanic Technol.*, 20(2003): 912-926.